JACS
JOURNAL OF THE AMERICAN CHEMICAL SOCIETY
pubs.acs.org/JACS
Communication

# Detection of a Geminate Photoproduct of Bovine Cytochrome *c* Oxidase by Time-Resolved Serial Femtosecond Crystallography

Izumi Ishigami, Sergio Carbajo, Nadia Zatsepin, Masahide Hikita, Chelsie E. Conrad, Garrett Nelson, Jesse Coe, Shibom Basu, Thomas Grant, Matthew H. Seaberg, Raymond G. Sierra, Mark S. Hunter, Petra Fromme, Raimund Fromme, Denis L. Rousseau,* and Syun-Ru Yeh*

Cite This: *J. Am. Chem. Soc.* 2023, 145, 22305−22309
Read Online
ACCESS | Metrics & More | Article Recommendations | Supporting Information

**ABSTRACT:** Cytochrome *c* oxidase (C*c*O) is a large membrane-bound hemeprotein that catalyzes the reduction of dioxygen to water. Unlike classical dioxygen binding hemeproteins with a heme *b* group in their active sites, C*c*O has a unique binuclear center (BNC) composed of a copper atom ($Cu_B$) and a heme $a_3$ iron, where $O_2$ binds and is reduced to water. CO is a versatile $O_2$ surrogate in ligand binding and escape reactions. Previous time-resolved spectroscopic studies of the CO complexes of bovine C*c*O (bC*c*O) revealed that photolyzing CO from the heme $a_3$ iron leads to a metastable intermediate ($Cu_B$-CO), where CO is bound to $Cu_B$, before it escapes out of the BNC. Here, with a pump-probe based time-resolved serial femtosecond X-ray crystallography, we detected a geminate photoproduct of the bC*c*O−CO complex, where CO is dissociated from the heme $a_3$ iron and moved to a temporary binding site midway between the $Cu_B$ and the heme $a_3$ iron, while the locations of the two metal centers and the conformation of Helix-X, housing the proximal histidine ligand of the heme $a_3$ iron, remain in the CO complex state. This new structure, combined with other reported structures of bC*c*O, allows for a clearer definition of the ligand dissociation trajectory as well as the associated protein dynamics.



Cytochrome *c* oxidase (C*c*O) is the terminal enzyme in the electron transfer chain in the inner membrane of mitochondria. It reduces dioxygen to two water molecules by accepting four electrons from cytochrome *c* and four protons from the negative side of the mitochondrial membrane. At the same time, it harnesses the chemical energy derived from the dioxygen reduction chemistry to translocate four protons from the negative to positive side of the membrane for the production of the electrochemical proton gradient required for ATP synthesis by ATP synthase.[1] To accomplish this complex task, C*c*O possesses four redox active centers, $Cu_A$, heme *a*, and a binuclear center (BNC) formed by a copper atom ($Cu_B$) and the heme $a_3$ iron,[2] where $O_2$ binds and is reduced to water. The dioxygen reduction reaction catalyzed by C*c*O has been extensively studied and is well-understood.[3−7] In contrast, the $O_2$ binding dynamics preceding the oxygen chemistry remains elusive as it is technically challenging to monitor the fleeting $O_2$ complex.

Carbon monoxide (CO), like $O_2$, is an excellent ligand for hemeproteins, but unlike $O_2$, it forms nonreactive complexes with them. Furthermore, when CO is bound to a heme iron, it is readily dissociable by a short pulse of visible light, making it a versatile tool for the investigation of ligand dissociation and rebinding dynamics.[8,9] Time-resolved Fourier-transform infrared spectroscopic studies at ambient temperatures showed that photolyzing CO from the heme $a_3$ iron in the BNC of bovine C*c*O (bC*c*O) in free solution leads to the formation of a characteristic $Cu_B$-CO intermediate (Figure 1A), where the photolyzed CO is coordinated to the $Cu_B$, in less than 1 ps.[10−14] The photolyzed CO subsequently disociates from $Cu_B$ and escapes out of the BNC in ∼1.5 $\mu$s[11,15] to generate the ligand-free reduced species (R). By extension, it is believed that the bimolecular binding reaction of CO, as well as $O_2$, follows the same trajectery, but in a reverse order, with $Cu_B$ as a temporary ligand stopping point.[6,16−18] In addition to the $Cu_B$-CO intermediate, transient UV−vis absorption spectroscopic data suggest that a geminate photoproduct, where CO has been photolyzed from heme $a_3$ iron but not yet coordinated to $Cu_B$, is formed immediately following CO photodissociation.[11,15] This proposed intermediate, however, has never been experimentally identified.

Crystallographic studies of the bC*c*O−CO complex showed that X-rays from synchrotron light sources, like visible light, can photolyze CO from heme $a_3$.[19] To prevent the X-ray induced radiation damage, we employed serial femtosecond crystallography (SFX)[20] to determine the structure of the intact bC*c*O−CO complex.[19] With SFX, the diffraction patterns of randomly oriented microcrystals suspended in an aqueous jet, which intersects the femtosecond pulses from an X-ray free-electron laser (XFEL), are sequentially collected and then merged for structural determination. As the radiation damage processes do not occur until after the termination of each ultrashort laser pulse, radiation damage-free structures

**Received:** July 20, 2023
**Published:** September 11, 2023

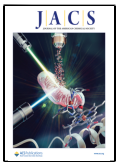

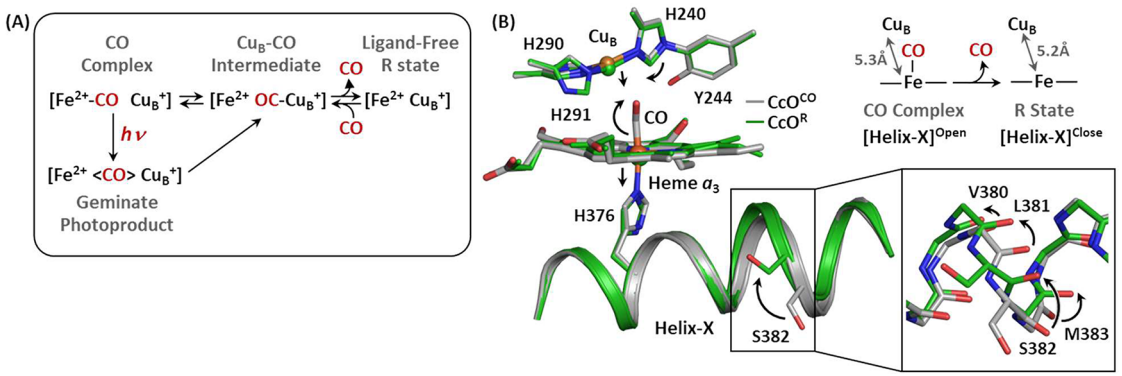


**Figure 1.** Proposed CO dissociation mechanism of bC*c*O (A) and the associated structural transition (B). The conformational changes induced by dissociation of CO from the CO complex (PDB ID: 5W97, gray) to generate the ligand-free R species (PDB ID: 7THU, green) are indicated by the arrows. The lower right inset shows the expanded view of the [380−383] fragment; the arrows indicate the rotation of the backbone carbonyl groups. The side chains, except that of S382, are not shown for clarity.

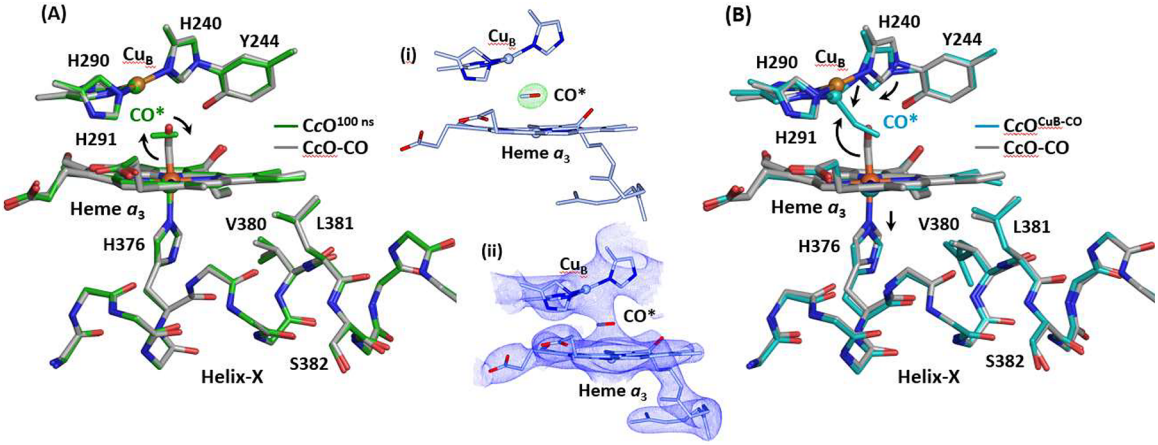


**Figure 2.** Structure of the geminate photoproduct of bC*c*O determined in this work (PDB ID: 8GBT, green) (A) with respect to the reported Cu$_B$-CO intermediate structure (PDB ID: 5X1B, cyan) (B). The structure of the CO complex (PDB ID: 5W97, gray) was shown as a reference in each panel to illustrate the CO dissociation induced structural changes, as indicated by the arrows. Inset (i) and (ii) show the $F_O$-$F_C$ difference map and the $2F_O$-$F_C$ map (with CO modeled in) of the BNC contoured at 6 and 2 $\sigma$, respectively.

can be obtained under native-like conditions at ambient temperatures.[20] The comparison of the SFX structure of the bC*c*O−CO complex with that of the ligand-free protein (R) (Figure 1B) shows that CO dissociation leads to the displacement of the Cu$_B$-H240 moiety toward the heme $a_3$ and the movement of the heme $a_3$ iron-H376 moiety away from the Cu$_B$ center. The structural changes to the BNC are associated with a conformational transition in the [380−383] fragment of Helix-X (housing H376), from an open to a closed conformation,[21] and a ∼ 120° flip of the S382 side chain.

To comprehend the protein dynamics associated with the CO dissociation reaction, here we sought to employ a time-resolved SFX method, using an OPO laser as the pump beam (to photolyze CO from the bC*c*O−CO complex) and a XFEL as the probe beam to determine the structure of the photoproduct populated at 100 ns following the initiation of the reaction. The plate-like bC*c*O−CO microcrystals (∼20 × 20 × 4 $\mu m^3$ in size) were prepared with a previously reported protocol.[19] A slurry of the microcrystals was loaded in a gastight syringe and injected into the XFEL beam as a thin (4 $\mu$m) solution jet in a vacuum chamber[22] (see Material and Methods in the Supporting Information). Each OPO laser pulse (with a width of ∼8 ns) was timed at 100 ns before the XFEL pulse (with a width of ≤40 fs). The wavelength and pulse energy of the OPO laser were set at 492 nm and 60 $\mu$J, respectively, to ensure that the CO was completely photolyzed. The serial diffraction patterns were collected for 85 min, among which 16,520 indexable patterns were merged and analyzed.

The initial structure was solved with molecular replacement using the structure of ligand-free reduced bC*c*O (PDB ID: 7THU) as the search model. In the $F_O$-$F_C$ difference map contoured at 6 $\sigma$ (see inset-i in Figure 2A), clear ligand electron density is evident between Cu$_B$ and heme $a_3$; in addition, there is no residual electron density connecting the ligand density to the heme $a_3$ iron (even when the map is contoured at 3$\sigma$), indicating that CO is completely photolyzed and that there is no geminate CO recombination (which is in good agreement with free solution reactions).[23] As the C and O atoms are indistinguishable in the current data, the ligand electron density was arbitrarily modeled with the atom closer to the iron assigned as the C atom (inset-ii). The final structure was refined to a resolution of 2.8 Å (PDB ID: 8GBT, see Supporting Information Table S1).

The structural data reveal that upon photodissociation the CO rotates ∼90° with respect to its center of mass, such that it lies parallel with the heme $a_3$ plane, midway between Cu$_B$ and the heme $a_3$ iron (Figure 2A). It is stabilized by sandwiching


https://doi.org/10.1021/jacs.3c07803
J. Am. Chem. Soc. 2023, 145, 22305−22309

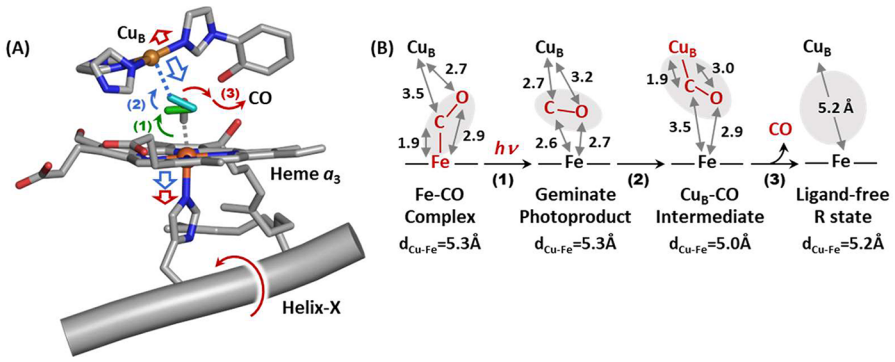


**Figure 3.** CO dissociation reaction trajectory in bC*c*O. (A) Schematic illustration of the 3-step reaction and (B) changes in the critical interatomic distances during the reaction.

between heme $a_3$ and Cu$_B$, as well as by H291, H240 and V243, via either van der Waals and/or electrostatic interactions (see Figure S1 in the Supporting Information). The Cu$_B$-H240 and heme $a_3$ iron-H376 moieties, as well as the conformation of Helix-X, remain unperturbed, indicating that the proten matrix does not relax to the ligand-free R state until later during the reaction.

The current structure is distinct from that of the photoproduct reported by Shimada et al. (PDB ID: 5X1B),[24] derived from a different pump−probe experiment, where CO is photolyzed from the heme $a_3$ iron and coordinated to Cu$_B$ (Figure 2B). With respect to the CO complex, the Cu$_B$ atom moved toward the heme $a_3$ by 0.5 Å, while the heme $a_3$ iron atom moved away from the heme plane by 0.2 Å, resulting in the contraction of the Cu$_B$-heme $a_3$ iron distance from 5.3 to 5.0 Å, but Helix-X remained in the CO-complex (open) state. The structural features of the two photoproducts, combined with the reaction scheme illustrated in Figure 1A, suggest that the intermediate reported in this work is the long-suspected primary geminate photoproduct, while the Shimada structure is the Cu$_B$-CO intermediate. It is important to note that the two photoproducts are distinct from that generated during X-ray diffraction data collection induced by constant synchrotron light illumination (PDB ID: 5WAU)[19] (see Figure S2 in the Supporting Information), as the latter represents a unique photostationary state, instead of a true reaction intermediate.

The availability of the structures of the two reaction intermediates of bC*c*O, combined with the equilibrium structures of the CO-complex and ligand-free R state, allows us to define the ligand dissociation trajectory and the associated protein dynamics, as depicted in Figure 3. The heme $a_3$ iron-CO bond scission first leads to the rotation of the CO to a new orientation parallel with the heme $a_3$ plane (step 1, indicated by the green arrow in Figure 3A), while the Cu$_B$-H240 and heme $a_3$ iron-H376 moieties and Helix-X remain in the CO-complex (open) state. Subsequently, CO further rotates toward Cu$_B$ to establish a coordination bond with it (step 2, blue arrows). It triggers the relaxation of the BNC to a ligand-free R-like conformation, resulting in a 0.3 Å contraction of the Cu$_B$-Fe distance, while the conformation of Helix-X remains unperturbed. Finally, CO dissociates from Cu$_B$ and escapes out of the BNC (step 3, red arrows), which is accompanied by a 0.2 Å re-expansion of the Cu$_B$-Fe distance and a structural transition of Helix-X to the equilibrium R (closed) conformation, thereby completing the reaction.

It is important to note that in free solution reactions CO was able to migrate to the Cu$_B$ site within 1 ps following the photolysis from heme $a_3$.[25,26] The current data indicate that the reaction taking place in the microcrystals is at least 4 orders of magnitude slower. It is in agreement with our previous data showing that the oxygen reaction catalyzed by bC*c*O is ∼10,000-fold slower in crystalline states as compared to that in solution phases.[27] They indicate that the crystal lattice constrains certain protein motions required for the protein to cross the activation energy barriers and call for computational studies to delineate the structural factors underlying the activation processes.

The overall protein structural transition induced by CO dissociation in bC*c*O is comparable to that in myoglobin (Mb), a model system considered as the hydrogen atom of biology.[28] Mb is a small water-soluble protein that contains a heme *b* group embedded in the protein matrix. The heme iron is coordinated by a histidine residue (H93) from Helix-F on the proximal side (equivalent to H376 in Helix-X in bC*c*O), and a diatomic ligand, such as $O_2$ or CO, on the distal side, which is stabilized by another histidine residue (H64) from Helix-E (in place of the Cu$_B$ moiety in bC*c*O). Photodissociation of CO from the Mb-CO complex leads to a geminate photoproduct, where CO rotates and translates to a nearby docking site, such that it lies parallel with the heme plane as in bC*c*O, within the distal heme pocket.[29] It is accompanied by the displacement of the heme iron out of the heme plane, as well as the concurrent movement of (i) the proximal H93 and the associated Helix-F away from the heme, and (ii) the distal H64 and the associated Helix-E toward the heme.[30−32] These structural changes near the active site then propagate to the rest of the protein matrix through a global protein relaxation in a quake-like motion to establish the final equilibrium ligand-free structure.[30−32]

Despite the similarities, the protein dynamics associated with CO dissociation in bC*c*O is much less cooperative compared to that in Mb. The dissociation of CO from the heme iron in bC*c*O, like that in Mb, first leads to the formation of a geminate photoproduct, with CO bound to a docking site within the distal heme pocket, but it does not introduce any immediate structural changes to the heme or the protein matrix surrounding it. The presence of Cu$_B$ in the BNC in bC*c*O reroutes the CO migration pathway, rendering an additional Cu$_B$-CO intermediate. It is not until the CO dissociates from Cu$_B$ that the proximal Helix-X relaxes to the final equilibrium in the R state.

The unique CO dissociation-induced protein dynamics in bC*c*O is accompanied by transient contraction of the BNC (see Figure 3B), which plausibly plays an important role in


https://doi.org/10.1021/jacs.3c07803
J. Am. Chem. Soc. 2023, 145, 22305−22309

guiding the unidirectional movement of the ligand out of the BNC, thereby accounting for the lack of geminate recombination in the reaction, in contrast to the ∼40% geminate recombination in the Mb reaction.[30] This characteristic protein plasticity in bC*c*O is conceivably critical for coupling the oxygen chemistry occurring in the BNC to proton translocation.

In summary, the data presented here provide the first direct evidence of the geminate photoproduct of bC*c*O. The definition of its structure, combined with a previously reported $Cu_B$-CO structure (PDB ID: 5X1B),[24] enables us to define the ligand dissociation trajectory, as well as the associated protein dynamics, more clearly for the first time. It offers exciting experimental blueprints for the computational interrogation of the energy landscape associated with the ligand migration reaction.

## ■ ASSOCIATED CONTENT

### Supporting Information

The Supporting Information is available free of charge at https://pubs.acs.org/doi/10.1021/jacs.3c07803.

Materials and methods, additional structural information, and crystallographic data collection and refinement statistics (PDF)

## ■ AUTHOR INFORMATION


### Corresponding Authors

**Denis L. Rousseau** − *Department of Biochemistry, Albert Einstein College of Medicine, Bronx, New York 10461, United States;* orcid.org/0000-0001-5405-5128; Email: denis.rousseau@einsteinmed.edu

**Syun-Ru Yeh** − *Department of Biochemistry, Albert Einstein College of Medicine, Bronx, New York 10461, United States;* orcid.org/0000-0002-9858-386X; Email: syun-ru.yeh@einsteinmed.edu

### Authors

**Izumi Ishigami** − *Department of Biochemistry, Albert Einstein College of Medicine, Bronx, New York 10461, United States;* orcid.org/0000-0001-6929-1908

**Sergio Carbajo** − *Linac Coherent Light Source, SLAC National Accelerator Laboratory, Menlo Park, California 94025, United States; Electrical and Computer Engineering Department and Physics and Astronomy Department, University of California Los Angeles, Los Angeles, California 90045, United States*

**Nadia Zatsepin** − *Department of Physics and Center for Applied Structural Discovery, The Biodesign Institute, Arizona State University, Tempe, Arizona 85287, United States; Chemistry and Physics, La Trobe University, Bundoora, VIC 3086, Australia*

**Masahide Hikita** − *Department of Biochemistry, Albert Einstein College of Medicine, Bronx, New York 10461, United States;* Present Address: Structural Biology Research Center, Institute of Materials Structure Science, High Energy Accelerator Research Organization, 1−1 Oho, Tsukuba, Ibaraki 305−0801 Japan

**Chelsie E. Conrad** − *Center for Applied Structural Discovery, The Biodesign Institute and School of Molecular Sciences, Arizona State University, Tempe, Arizona 85287, United States;* Present Address: Center for Genomic Medicine, University of Utah, 30 South 2000 East, Salt Lake City, UT 84112, United States

**Garrett Nelson** − *Department of Physics, Arizona State University, Tempe, Arizona 85287, United States;* Present Address: Boeckeler Instruments, Inc. 4650 S Butterfield Dr, Tucson, AZ 85714, United States

**Jesse Coe** − *Center for Applied Structural Discovery, The Biodesign Institute and School of Molecular Sciences, Arizona State University, Tempe, Arizona 85287, United States;* Present Address: KBI Biopharma, 1101 Hamlin Rd, Durham, NC 27704, United States

**Shibom Basu** − *Center for Applied Structural Discovery, The Biodesign Institute and School of Molecular Sciences, Arizona State University, Tempe, Arizona 85287, United States;* Present Address: EMBL Grenoble, 71 Avenue des Martyrs, CS 90181, 38042 Grenoble, France

**Thomas Grant** − *Department of Structural Biology, University of Buffalo, Buffalo, New York 14203, United States;* orcid.org/0000-0002-8583-3700

**Matthew H. Seaberg** − *Linac Coherent Light Source, SLAC National Accelerator Laboratory, Menlo Park, California 94025, United States*

**Raymond G. Sierra** − *Linac Coherent Light Source, SLAC National Accelerator Laboratory, Menlo Park, California 94025, United States*

**Mark S. Hunter** − *Linac Coherent Light Source, SLAC National Accelerator Laboratory, Menlo Park, California 94025, United States*

**Petra Fromme** − *Center for Applied Structural Discovery, The Biodesign Institute and School of Molecular Sciences, Arizona State University, Tempe, Arizona 85287, United States*

**Raimund Fromme** − *Center for Applied Structural Discovery, The Biodesign Institute and School of Molecular Sciences, Arizona State University, Tempe, Arizona 85287, United States*

Complete contact information is available at: https://pubs.acs.org/10.1021/jacs.3c07803


### Author Contributions

The manuscript was written through contributions of all authors.

### Notes

The authors declare no competing financial interest.

## ■ ACKNOWLEDGMENTS

The SFX experiments were carried out at the Linac Coherent Light Source (LCLS) at the SLAC National Accelerator Laboratory. LCLS is an Office of Science User Facility operated for the US Department of Energy Office of Science by Stanford University. Use of the LCLS, SLAC National Accelerator Laboratory, is supported by the US Department of Energy, Office of Science, Office of Basic Energy Sciences, under Contract DE-AC02-76SF00515. Parts of the sample delivery system used at LCLS for this research were funded by NIH Grant P41GM103393, formerly P41RR001209. This work was supported by National Science Foundation (NSF) grants CHE-1404929 (to D.L.R. and S.-R.Y.), ABI Innovations Award 1565180 (to N.A.Z.) and Science and Technology Center Award 1231306. This work was also supported by National Institutes of Health (NIH) grants GM126297 (D.L.R. and S.-R.Y.), GM115773 (S.-R.Y.), GM095583 (to P.F.), S10 OD023453 and P41 GM139687, as well as the

Biodesign Center for Applied Structural Discovery at Arizona State University.

## ■ ABBREVIATIONS

C*c*O, cytochrome *c* oxidase; bC*c*O, bovine cytochrome *c* oxidase; Mb, myoglobin; BNC, binuclear center; CO, carbon monoxide; SFX, serial femtosecond crystallography; GDVN, gas dynamic virtual nozzle; LCLS, Linac Coherent Light Source

## ■ REFERENCES

(1) Wikstrom, M.; Krab, K.; Sharma, V. Oxygen Activation and Energy Conservation by Cytochrome c Oxidase. *Chem. Rev.* **2018**, *118* (5), 2469−2490.
(2) Yoshikawa, S.; Shimada, A. Reaction mechanism of cytochrome C oxidase. *Chem. Rev.* **2015**, *115* (4), 1936−1989.
(3) Han, S.; Takahashi, S.; Rousseau, D. L. Time dependence of the catalytic intermediates in cytochrome c oxidase. *J. Biol. Chem.* **2000**, *275* (3), 1910−1919.
(4) Kitagawa, T.; Ogura, T. Time-resolved resonance Raman investigation of oxygen reduction mechanism of bovine cytochrome c oxidase. *Journal of bioenergetics and biomembranes* **1998**, *30* (1), 71−79.
(5) Wikstrom, M.; Gennis, R. B.; Rich, P. R. Structures of the intermediates in the catalytic cycle of mitochondrial cytochrome c oxidase. *Biochim Biophys Acta Bioenerg* **2023**, *1864* (2), 148933.
(6) Varotsis, C.; Zhang, Y.; Appelman, E. H.; Babcock, G. T. Resolution of the reaction sequence during the reduction of O2 by cytochrome oxidase. *Proc. Natl. Acad. Sci. U.S.A.* **1993**, *90* (1), 237−241.
(7) Belevich, I.; Verkhovsky, M. I. Molecular mechanism of proton translocation by cytochrome c oxidase. *Antioxid Redox Signal* **2008**, *10* (1), 1−29.
(8) Austin, R. H.; Beeson, K. W.; Eisenstein, L.; Frauenfelder, H.; Gunsalus, I. C. Dynamics of ligand binding to myoglobin. *Biochemistry* **1975**, *14* (24), 5355−5373.
(9) Gibson, Q. H.; Greenwood, C. Reactions of cytochrome oxidase with oxygen and carbon monoxide. *Biochem. J.* **1963**, *86* (3), 541−554.
(10) Alben, J. O.; Moh, P. P.; Fiamingo, F. G.; Altschuld, R. A. Cytochrome oxidase (a3) heme and copper observed by low-temperature Fourier transform infrared spectroscopy of the CO complex. *Proc. Natl. Acad. Sci. U. S. A.* **1981**, *78* (1), 234−237.
(11) Dyer, R. B.; Einarsdottir, O.; Killough, P. M.; Lopez-Garriga, J. J.; Woodruff, W. H. Transient binding of photodissociated carbon monoxide to CuB+ of eukaryotic cytochrome oxidase at ambient temperature. Direct evidence from time-resolved infrared spectroscopy. *J. Am. Chem. Soc.* **1989**, *111* (19), 7657−7659.
(12) Stoutland, P. O.; Lambry, J. C.; Martin, J. L.; Woodruff, W. H. Femtosecond dynamics of reduced cytochrome oxidase and its CO derivative. *J. Phys. Chem.* **1991**, *95* (17), 6406−6408.
(13) Dyer, R. B.; Peterson, K. A.; Stoutland, P. O.; Woodruff, W. H. Picosecond infrared study of the photodynamics of carbonmonoxy-cytochrome c oxidase. *Biochemistry* **1994**, *33* (2), 500−507.
(14) Dyer, R. B.; Peterson, K. A.; Stoutland, P. O.; Woodruff, W. H. Ultrafast photoinduced ligand transfer in carbonmonoxy cytochrome c oxidase. Observation by picosecond infrared spectroscopy. *J. Am. Chem. Soc.* **1991**, *113* (16), 6276−6277.
(15) Woodruff, W. H.; Einarsdottir, O.; Dyer, R. B.; Bagley, K. A.; Palmer, G.; Atherton, S. J.; Goldbeck, R. A.; Dawes, T. D.; Kliger, D. S. Nature and functional implications of the cytochrome a3 transients after photodissociation of CO-cytochrome oxidase. *Proc. Natl. Acad. Sci. U.S.A.* **1991**, *88* (6), 2588−2592.
(16) Blackmore, R. S.; Greenwood, C.; Gibson, Q. H. Studies of the primary oxygen intermediate in the reaction of fully reduced cytochrome oxidase. *J. Biol. Chem.* **1991**, *266* (29), 19245−19249.
(17) Oliveberg, M.; Malmstrom, B. G. Reaction of dioxygen with cytochrome c oxidase reduced to different degrees: indications of a transient dioxygen complex with copper-B. *Biochemistry* **1992**, *31* (14), 3560−3563.
(18) Woodruff, W. H. Coordination dynamics of heme-copper oxidases. The ligand shuttle and the control and coupling of electron transfer and proton translocation. *J. Bioenerg Biomembr* **1993**, *25* (2), 177−188.
(19) Ishigami, I.; Zatsepin, N. A.; Hikita, M.; Conrad, C. E.; Nelson, G.; Coe, J. D.; Basu, S.; Grant, T. D.; Seaberg, M. H.; Sierra, R. G.; et al. Crystal structure of CO-bound cytochrome c oxidase determined by serial femtosecond X-ray crystallography at room temperature. *Proc. Natl. Acad. Sci. U. S. A.* **2017**, *114* (30), 8011−8016.
(20) Boutet, S.; Lomb, L.; Williams, G. J.; Barends, T. R.; Aquila, A.; Doak, R. B.; Weierstall, U.; DePonte, D. P.; Steinbrener, J.; Shoeman, R. L.; et al. High-resolution protein structure determination by serial femtosecond crystallography. *Science* **2012**, *337* (6092), 362−364.
(21) Ishigami, I.; Zatsepin, N. A.; Hikita, M.; Conrad, C. E.; Nelson, G.; Coe, J. D.; Basu, S.; Grant, T. D.; Seaberg, M. H.; Sierra, R. G.; et al. Crystal structure of CO-bound cytochrome c oxidase determined by serial femtosecond X-ray crystallography at room temperature. *Proc. Natl. Acad. Sci. U.S.A.* **2017**, *114* (30), 8011−8016.
(22) DePonte, D. P.; Weierstall, U.; Schmidt, K.; Warner, J.; Starodub, D.; Spence, J. C. H.; Doak, R. B. Gas dynamic virtual nozzle for generation of microscopic droplet streams. *J. Phys. D: Appl. Phys.* **2008**, *41* (19), 195505.
(23) Findsen, E. W.; Centeno, J.; Babcock, G. T.; Ondrias, M. R. Cytochrome a3 hemepocket relaxation subsequent to ligand photolysis from cytochrome oxidase. *J. Am. Chem. Soc.* **1987**, *109* (18), 5367−5372.
(24) Shimada, A.; Kubo, M.; Baba, S.; Yamashita, K.; Hirata, K.; Ueno, G.; Nomura, T.; Kimura, T.; Shinzawa-Itoh, K.; Baba, J.; et al. A nanosecond time-resolved XFEL analysis of structural changes associated with CO release from cytochrome c oxidase. *Science advances* **2017**, *3* (7), e1603042.
(25) Vos, M. H.; Liebl, U. Time-resolved infrared spectroscopic studies of ligand dynamics in the active site from cytochrome c oxidase. *Biochimica et biophysica acta* **2015**, *1847* (1), 79−85.
(26) Einarsdottir, O.; Dyer, R. B.; Lemon, D. D.; Killough, P. M.; Hubig, S. M.; Atherton, S. J.; Lopez-Garriga, J. J.; Palmer, G.; Woodruff, W. H. Photodissociation and recombination of carbonmonoxy cytochrome oxidase: dynamics from picoseconds to kiloseconds. *Biochemistry* **1993**, *32* (45), 12013−12024.
(27) Ishigami, I.; Lewis-Ballester, A.; Echelmeier, A.; Brehm, G.; Zatsepin, N.; Grant, T.; Jesse Coe, J.; Lisova, S.; Nelson, G.; Zhang, S.; et al. Snapshot of an Oxygen Intermediate in the Catalytic Reaction of Cytochrome c Oxidase. *Proc. Nat. Acad. Sci. (USA)* **2019**, *116* (9), 3572−3577.
(28) Frauenfelder, H.; McMahon, B. H.; Fenimore, P. W. Myoglobin: the hydrogen atom of biology and a paradigm of complexity. *Proc. Natl. Acad. Sci. U. S. A.* **2003**, *100* (15), 8615−8617.
(29) Chu, K.; Vojtchovsky, J.; McMahon, B. H.; Sweet, R. M.; Berendzen, J.; Schlichting, I. Structure of a ligand-binding intermediate in wild-type carbonmonoxy myoglobin. *Nature* **2000**, *403* (6772), 921−923.
(30) Srajer, V.; Teng, T.; Ursby, T.; Pradervand, C.; Ren, Z.; Adachi, S.; Schildkamp, W.; Bourgeois, D.; Wulff, M.; Moffat, K. Photolysis of the carbon monoxide complex of myoglobin: nanosecond time-resolved crystallography. *Science* **1996**, *274* (5293), 1726−1729.
(31) Ansari, A.; Berendzen, J.; Bowne, S. F.; Frauenfelder, H.; Iben, I. E.; Sauke, T. B.; Shyamsunder, E.; Young, R. D. Protein states and proteinquakes. *Proc. Natl. Acad. Sci. U. S. A.* **1985**, *82* (15), 5000−5004.
(32) Barends, T. R.; Foucar, L.; Ardevol, A.; Nass, K.; Aquila, A.; Botha, S.; Doak, R. B.; Falahati, K.; Hartmann, E.; Hilpert, M.; et al. Direct observation of ultrafast collective motions in CO myoglobin upon ligand dissociation. *Science* **2015**, *350* (6259), 445−450.


https://doi.org/10.1021/jacs.3c07803
J. Am. Chem. Soc. 2023, 145, 22305−22309